RSC Advances

PAPER

View Article Online
View Journal | View Issue

Cite this: *RSC Adv.*, 2023, **13**, 11938

Copper-doped perylene diimide supramolecules combined with TiO_2 for efficient photoactivity†

Yu Liang, Wanrui Gui, Zhihong Yang, Kang Cheng, Xin Zhou, Can Yang, Jianmei Xu and Wei Zhou *

Designing organic–inorganic hybrid semiconductors is an effective strategy for improving the performance of the photocatalyst under visible light irradiation. In this experiment, we firstly introduced Cu into perylenediimide supramolecules (PDIsm) to prepare the novel Cu-dopped PDIsm (CuPDIsm) with one-dimensional structure and then incorporated CuPDIsm with TiO_2 to improve the photocatalytic performance. The introduction of Cu in PDIsm increases both the visible light adsorption and specific surface areas. Cu^{2+} coordination link between adjacent perylenediimide (PDI) moleculars and H-type π–π stacking of the aromatic core greatly accelerate the electron transfer in CuPDIsm system. Moreover, the photo-induced electrons generated by CuPDIsm migrate to TiO_2 nanoparticles through hydrogen bond and electronic coupling at the TiO_2/CuPDIsm heterojunction, which further accelerates the electron transfer and the separation efficiency of the charge carriers. So, the TiO_2/CuPDIsm composites exhibit excellent photodegradation activity under visible light irradiation, reaching the maximum values of 89.87 and 97.26% toward tetracycline and methylene blue, respectively. This study provides new prospects for the development of metal-dopping organic systems and the construction of inorganic–organic heterojunctions, which can effectively enhance the electron transfer and improve the photocatalytic performance.

Received 13th February 2023
Accepted 6th April 2023

DOI: 10.1039/d3ra00965c

rsc.li/rsc-advances

1. Introduction

Photocatalytic technology is environmentally friendly for organic pollutants degradation, hydrogen evolution and photo-oxidation synthesis under sunlight irradiation.[1,2] It is well known that semiconductor photocatalysts play a key role to improve the photocatalytic efficiency, implying that the pursuit of high-quality photocatalysts remains a research priority in the field of photocatalysis.[3–5]

Perylene diimide (PDI) organic materials and their derivatives, often synthesized by solution method under N_2 or Ar inert atmosphere conditions, have many merits, such as good electron-accepting character,[6,7] high mobility,[8] wide light response wavelength[9] and outstanding photochemical stability,[10] so they are the potential candidates for photocatalytic applications.[11–13] PDI as a n-type organic semiconductor can be used as an independent catalyst in photocatalytic process, but its photocatalytic efficiency is low due to its electron-deficient π-conjugated cores, rapid charge recombination and inefficient charge transport molecular system.[14,15] To solve these problems, some effective strategies were employed to enhance the photocatalytic activity, for instance, designing PDI molecula,[16] adjusting supramolecular configuration,[6,17] coupling with other photocatalysts or cocatalysts,[18–21] *etc.*

In fact, incorporating PDI assembles with other photocatalysts or cocatalysts is the usual method, which constructs powerful photocatalytic systems with improved photoinduced electron transfer. For example, PDI/g-C_3N_4 showed the enhanced electron delocalization effect and the interfacial charge transfer with the formation of n–n heterojunction system.[10] PDI coupling with WO_3 (ref. 22), BiOCl[23] and Ag_3PO_4 (ref. 24) had high photoactivity arisen from the efficient carriers separation and the formation of Z-scheme heterojunction. PDI/TiO_2 composites showed the improved photoactivity due to the electrons transporting from PDI to the conduction band of TiO_2.[15,25,26] PDI/Pd composites had high electron transfer efficiency due to two opposite types of electron transfer pathway.[7] PTCDI self-assembled with C_{60} lowered the position of valence band, narrowed the band gap and promoted the transfer of the photogenerated carriers.[27] In PDI/Graphene system, graphene quantum dots (GQDs) contributed to the electrons delocalization *via* π–π action with PDI and promoted electron transfer from GQDs to PDI.[28]

Recently, it is found that the doping of Zn and Co can facilitate fascinating modification of PDI supramolecules through π–π stacking of the organized PDI rings and the metal

Faculty of Materials Science and Chemistry, Engineering Research Center of Nano-Geomaterials of Ministry of Education, China University of Geosciences, Wuhan, 430074, China. E-mail: weizhou@cug.edu.cn; Tel: +86-27-67884991

† Electronic supplementary information (ESI) available. See DOI: https://doi.org/10.1039/d3ra00965c

bridging between the side chains of adjacent PDI moleculars.[29,30] The synergistic effects between the PDI arrays and metal sites provide the promising way for developing ideal photocatalysts toward the better utilization of solar energy.[31] However, to our knowledge, the incorporation of the metals into PDI supramolecules except Zn and Co have not been involved and how to introduce more types of metals into PDI assembles remain a great challenge.

In this work, we firstly designed a simple solvothermal method to prepare PDI, different from the conventional synthesis method of PDI under N_2 or Ar inert atmosphere conditions. To keep the consecutive and rapid photo-induced electron transfer process, we prepared Cu-doping PDI supramolecular (CuPDIsm) by the self-assembly of PDI moleculars in copper salt solution and then combined CuPDIsm with TiO_2 nanoparticles by solvothermal synthesis method, aiming for designing a novel CuPDIsm/TiO_2 photocatalysts with low-cost and excellent visible-light photocatalytic performance. Furthermore, we systematically elucidated the effect of Cu-bridging and TiO_2 coupling on the electron transfer process and the photocatalytic activity of the PDI supramoleculars.

2. Experimental

2.1 Materials

Perylene-3,4,9,10-tetracarboxylic dianhydride, glycine, imidazole, tetracycline (TC), methylene blue (MB), and methyl orange (MO) were purchased from Aladdin. Triethylamine, hydrochloric acid, copper nitrate trihydrate, tetrabutyl titanate, glacial acetic acid, sodium hydroxide and *N*,*N*-dimethylformamide (DMF) were purchased from Sinopharm Chemical Reagent Co. All reagents were analytically pure and could be used without further purification.

2.2 Synthesis of crude PDI

Different from the conventional preparing method of PDI under N_2 or Ar inert atmosphere conditions, we have designed a solvothermal method to prepare PDI, which has many merits like convenient operation, good effect and low cost. Firstly, 1.4 g of perylene-3,4,9,10-tetracarboxylic dianhydride and 2.6 g of glycine were well mixed and then 25 g of imidazole was added as the solvent. The obtained mixture was put in a reactor and heated at 110 °C for 5 h. After cooling, 50 mL of anhydrous ethanol and 80 mL of 3 M hydrochloric acid were sequentially added with continually stirring. Finally, the precipitate was collected through centrifugation and washed with ethanol and deionized water for 3 times, respectively. After being freeze-dried, crude PDI powder with bright red color was obtained.

2.3 Synthesis of PDIsm and CuPDIsm

200 mL of deionized water, 0.834 mL of triethylamine and 1 mL of 2 M NaOH solution were uniformly mixed. Then 0.54 g of crude PDI product was added with continually stirring for 1 h until PDI powders were fully dissolved and subsequently 27.3 mL of 4 M hydrochloric acid was added with rapidly stirring. Soon, flocculent precipitates were collected with centrifugation and washed with ethanol to get the dark red PDIsm products.

400 mg of crude PDI sample, 300 mg of $Cu(NO_3)_2 \cdot 3H_2O$ and 480 mg of NaOH were homogenously mixed, then 40 mL of DMF and 110 mL of deionized water were added with stirring. The mixture was put into a reactor and heated at 110 °C for 3 days. After cooling, centrifugation, washing and freeze-drying, CuPDIsm powders were obtained.

2.4 Synthesis of TiO_2/PDIsm and TiO_2/CuPDIsm

Firstly, 10 mL of tetrabutyl titanate was thoroughly mixed with 40 mL of anhydrous ethanol, followed by the addition of 4 mL of glacial acetic acid. Then 10 mL of ethanol solution ($V_{water}/V_{ethanol} = 2:3$) was slowly added with continuous stirring at 40 °C for 1 h to obtain TiO_2 precursor solution. Subsequently, 1 wt% PDIsm or CuPDIsm suspensions were mixed with the TiO_2 precursor solution with continuously stirring at 70 °C for 4 h, followed by the aging at room temperature for 12 h. Finally, the mixture was transferred into a reactor and heated at 180 °C for 5 h. After cooling, centrifugation, washing and freeze-drying, TiO_2/PDIsm and TiO_2/CuPDIsm composites were obtained.

2.5 Characterization

The crystal structure of the as prepared samples was analyzed by X-ray diffraction (XRD, Rigaku, Smartlab diffractometer). The specific surface area was evaluated using N_2 adsorption–desorption experiments with a Micromeritics SSA-7000 instrument. The morphology of the samples was examined by emission-scanning electron microscopy (SEM, Hitachi SU8010) equipped with X-ray energy dispersive spectrometer and transmission electron microscopy (TEM, JEOL2100F). UV-visible absorption spectra and diffuse reflectance spectra (DRS mode) were obtained using the UV-2600 spectrophotometer. The structure analysis was studied by a Fourier transform infrared spectrometer (FTIR, Nicolet iS50, America) and X-ray photoelectron spectroscopy (XPS, Thermo Fischer ESCALAB Xi+). Photoluminescence spectroscopy (PL) measurements were conducted on a Hitachi F-4500 fluorescence spectrometer and zeta potential measurements were carried out in neutral aqueous solution using Zetasizer Nano ZS90 device. Electrochemical analysis was performed on a CHI 660D workstation with 0.1 M Na_2SO_4 aqueous solution as the electrolyte solution.

2.6 Photocatalytic performance evaluation

Tetracycline, methylene blue and methyl orange were selected as target pollutants and the photocatalytic activity of photocatalyst samples was evaluated under visible light irradiation. A 300W xenon light lamp was used as an irradiation source with a distance of 10 cm between the solution and the lamp. 20 mg of the prepared catalyst was dispersed in 40 mL of a solution containing TC (10 mg L^{-1}), MO (50 mg L^{-1}) or MB (50 mg L^{-1} or 150 mg L^{-1}). Prior to irradiation, dark adsorption treatment was first carried out by magnetically stirring for 30 min to establish the adsorption–desorption equilibrium. Then 3 mL of the suspension was collected and filtered at given intervals of time during the light illumination. The filtrates were analyzed by UV-

vis spectrophotometer for TC at 358 nm, MO at 463 nm and MB at 664 nm.

3. Results and discussion

3.1 The organization and morphology investigation

The π–π stacking and crystal structure of self-assembled PDI supramoleculars can be revealed from UV-vis absorption spectra and XRD patterns, respectively.[31,32] The UV-vis absorption spectra of PDI monomer solution, PDIsm and CuPDIsm suspensions are shown in Fig. 1a. The spectrum of PDI dissolved in ethanol solution ($V_{water}/V_{ethanol} = 1:1$) shows three pronounced peaks in the range of 400–600 nm, which is attributed to the 0–0, 0–1 and 0–2 electronic transitions of monomeric PDI molecules.[33,34] Compared with PDI monomer, PDIsm dispersion shows broaden peaks with a blue-shift, indicating the H-type stacking between the PDI skeletons. CuPDIsm suspensions show an obvious blue-shift of the maximum peak as comparsion with PDI monomer, so it also has the H-type stacking structure. Moreover, in the spectrum of CuPDIsm, the absorbance intensity of the 0–1 vibronic transition peak at 504 nm is higher than the 0–0 transition peak at 543 nm, which is a typical indication of H-type aggregatio.[35,36] Therefore, the as prepared PDIsm and CuPDIsm have H-type π–π stacking structures, different from other metal-PDI supramoleculars with J-type aggregation structure in the literature.[29,30]

Fig. 1b shows the XRD patterns of PDIsm, CuPDIsm, TiO_2 and their composite samples. For the obtained PDIsm, the diffraction peaks between 24°–28° are generally considered to be the typical characteristic peaks of π–π stacking structures between PDI skeletons molecules, with the stacking layer spacing of 3.27–3.71 Å. This ordered π–π stacking contributes to long-range electron delocalization and the migration of photogenerated electrons along the π–π superposition direction,[33,36] which can enhance the electronic coupling[34,37] and charge mobility.[38] For the as prepared TiO_2, the peaks at 2θ = 25.3°, 37.8°, 48.1°, 54.9° and 62.7° are corresponding to the (101), (004), (200), (211), and (204) planes of anatase phase, respectively. For TiO_2/PDIsm composites, all the peaks can be detected in the spectra of PDI and TiO_2, implying that PDI supermolecules are integrated with TiO_2 without changing the crystal structure. For CuPDIsm, the intensity of the diffraction peaks is low as comparison with the spectrum of PDIsm, indicating that Cu doping hardly changes the crystal phase, but lowers the crystallinity of the PDI aggregates.

The morphology of the samples was analyzed by SEM and TEM. In Fig. S1a,† it can be seen that TiO_2 nanoparticles with the particle size of about 20–30 nm show heavy agglomerations due to the strong surface polarity. PDIsm and CuPDIsm show a clustered nanorod-like morphology with the diameter of less than 50 nm (Fig. S1b and c†). The nanorod shape of CuPDIsm is also observed in TEM image (Fig. 1c). This one-dimension structure originates from the self-assembly of carboxyl-containing perylene diimide molecules through intrinsic π-stacking of the aromatic core along the long axis and the hydrogen bond link between the carboxylic side chains along the short axis.[14,33] The hydrogen bond between the side chains of the adjacent PDI moleculars is replaced by metal–ligand interaction in CuPDIsm. For TiO_2/PDIsm and TiO_2/CuPDIsm (Fig. S1d and e†), TiO_2 particles are successfully distributed on the surface of PDIsm and CuPDIsm nanorods. Element

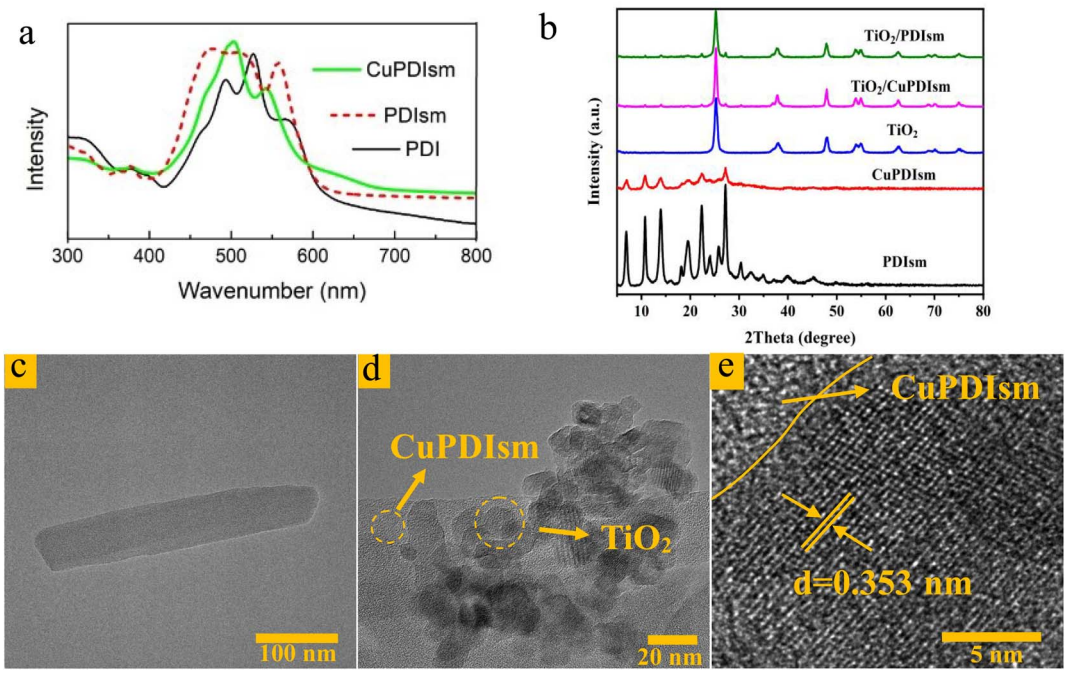

Fig. 1 UV-vis absorption spectra of PDI monomer solution and PDI supramolecular suspensions (a), XRD patterns of TiO_2, PDIsm, CuPDIsm and their composite samples (b), TEM images of CuPDIsm (c) and TiO_2/CuPDIsm (d), HRTEM of TiO_2/CuPDIsm (e).

mapping images (Fig. S2†) show that the presence of Cu element identifies the successful doping of Cu in PDIsm. The homogenous distribution of C, N, O and Ti indicates the good incorporation of TiO_2 with CuPDIsm. In addition, TEM images of TiO_2/CuPDIsm composites (Fig. 1c–e) show that TiO_2 nanoparticles are immobilized on the surface of CuPDIsm nanorods and the crystal plane spacing of 0.353 nm is corresponding to the highly reactive (101) plane of TiO_2 crystals. The close contact of TiO_2 with PDIsm and CuPDIsm indicates the formation of heterojunction interface, offering a direct pathway for photoelectron transport.

N_2 adsorption–desorption isotherms were employed to evaluate the specific surface area of the samples (Fig. S3a–c†). The isotherm plots of all samples belong to the IV type in the classification. Compared with PDIsm, CuPDIsm has much more mesopores and higher specific surface areas, which may be responsible for its lower crystallinity degree as discussed above in XRD results. The incorporation of PDIsm and TiO_2 further increases the mesopores and specific surface areas, so both Cu-doping and TiO_2-coupling can enhance the adsorption and reduce the migration distance of electrons from inside to the surface.

Fig. 2a shows FTIR spectra of the samples. The spectrum of CuPDIsm is similar to that of PDIsm, so the doping of Cu hardly affects the chemical structure of PDI supermolecules. The typical characteristic peak of PDIsm at 1695 cm^{-1} is corresponding to the stretching vibrations of the C=O bond of the PDI molecule,[21] which is attributed to the presence of carboxyl group at the side chains of PDI molecular. But this peak slightly shifts to 1697 cm^{-1} in the spectrum of CuPDIsm, which may be ascribed to the electrostatic interaction between carboxyl and Cu^{2+}.[25] Such blue shift verifies that PDI molecular interconnects each other through hydrogen bonds for PDIsm and Cu bridging for CuPDIsm along the short axis of the one-dimension supramoleculars. The Cu bridging is often in the way of metal–ligand interaction with one Cu^{2+} ion coordinated by three monodentate carboxylic groups from three deprotonated PDI ligands and one water molecule,[25] as shown in Fig. 2b. In the spectra of TiO_2/PDIsm and TiO_2/CuPDIsm, C=O peak also shifts to 1697 cm^{-1}, which may be due to the formation of hydrogen bonds between carboxyl group of the PDI molecule and –OH group of TiO_2 surface.[26,34,42–45] To further illustrate the interaction between Cu and PDI, Raman spectrum measurements were performed. As shown in the Fig. S4,† the characteristic bands in PDIsm are observed at 1292 cm^{-1} and 1369 cm^{-1} corresponding to C–H bending vibrations, and at 1572 cm^{-1} corresponding to C–C/C=C stretching vibration in perylene core.[39–41] Compared with Raman spectrum of PDIsm, these bands with stronger intensity in CuPDIsm slightly shift to the left, which may be attributed to Cu bonding between adjacent PDI units.

XPS characterization was used to study the surface chemistry of materials (Fig. 3a–f). In Fig. 3a, compared with PDIsm, CuPDIsm has a small new peak corresponding to Cu 2p signal, identifying the presence of Cu in this composite. The C 1s spectrum of PDIsm shows four peaks at 284.7, 286.1, 287.8 and 289.2 eV, representing C=C, C–N, C=O bonding and π-electron excitation, respectively, suggesting the formation of a self-assembled π-stacking structure. The O 1s spectrum of PDIsm shows three characteristic peaks at 531.6, 532.5 and 533.3 eV, related to C=O bond, C–O bond and adsorbed oxygen, respectively. Compared with PDIsm, CuPDIsm show a slight shift of C=O and C–O peaks to high binding energy, which is attributed to the formation of C–O–Cu interaction between adjacent PDI moleculars, further implying that CuPDIsm has a linear edge-to-edge organization through metal–ligand interaction along the short axis. An obvious blue shift of C=O and C–O peaks is detected in TiO_2/CuPDIsm, which may be due to the formation of the –C=O–H hydrogen bond and C–O–Ti bond at the heterojunction interface.[27] Such hydrogen bond and electronic coupling arisen from the interaction between surface carboxyl groups at PDI molecular side chain and the surface hydroxyl groups and unsaturated dangling bonds on TiO_2 particle, providing the fast passage for the electron transfer, as shown in Fig. 4.

In Ti 2p spectra (Fig. 3d), TiO_2 has two peaks at about 529.36 and 530.5 eV, corresponding to Ti–O bond and the surface hydroxyl groups (Ti–OH bond), respectively.[46] Notably, these two peaks in TiO_2/CuPDIsm shift to lower binding energy position, indicating that the surface electron density of TiO_2 increases.[24,47] This increasing surface electrons of TiO_2 originates from the transfer of electrons from CuPDIsm to TiO_2 through hydrogen bonds and C=O–Ti at the heterojunction

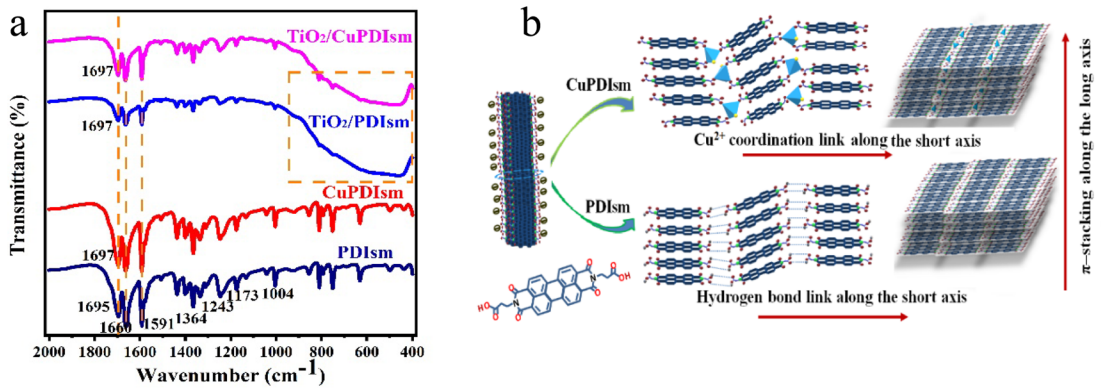

Fig. 2 FTIR spectra of the samples (a), self-assemble illustration of adjacent PDI molecular *via* hydrogen bond or tetra-coordinated interactions (b).

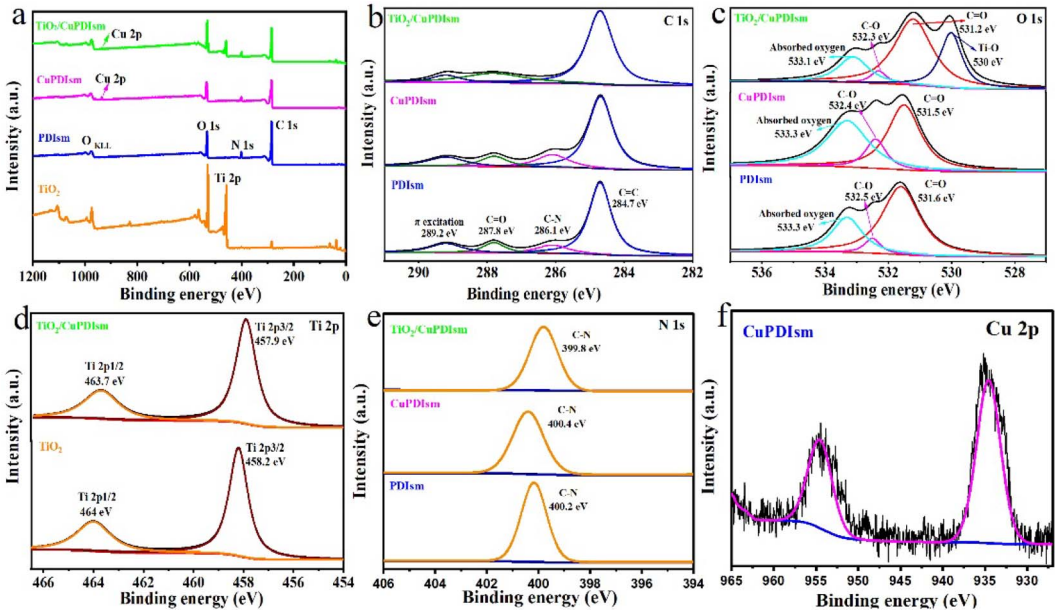

Fig. 3 XPS spectra of PDIsm, CuPDIsm and TiO_2/CuPDIsm samples. Survey scan (a) and fine scan energy spectra of C 1s (b), O 1s (c), Ti 2p (d), N 1s (e) and Cu 2p (f).

interface.[45] For N 1s pattern in Fig. 3e, a single high-intensity peak presents at 400.2 eV in PDIsm, corresponding to C–N bond. A small shift of this peak is detected in CuPDIsm (400.4 eV) and TiO_2/CuPDIsm (399.8 eV), indicating that the chemical environment of N 1s changed after PDIsm was dopped with Cu and coupled with TiO_2.[48] The Cu 2p spectrum (Fig. 3f) exhibits that two major peaks at 934.6 and 954.6 eV are ascribed to Cu $2p_{3/2}$ and Cu $2p_{1/2}$ valence states, respectively, confirming the presence of Cu as Cu^{2+} oxidation state[49] in CuPDIsm.

3.2 Photoelectric properties

The UV-vis absorption spectra of the samples were measured to explore the light-absorption ability (Fig. 5a). TiO_2 exhibits high absorption intensity in the UV region but low absorption ability in the visible region. In contrast, PDIsm has a weaker absorption of UV light, but strong response in the visible region of 400–700 nm. There are two absorption bands at 498 and 550 nm in the PDIsm, corresponding to the electronic transition in the isolated molecule and the π-electron delocalization between PDI chromophores, respectively.[7] It is noteworthy that the introduction of Cu into PDIsm greatly increases the absorption ability and causes the red-shift of absorption edge. The loading of TiO_2 nanoparticles onto PDIsm surface is also advantageous to increasing the light absorption of PDI self-assembly. So both Cu-dopped and TiO_2 coupling would enhance the photocatalytic performance of PDIsm under visible light irradiation. The band gap (E_g) of the as-prepared samples were estimated by Tauc's plot. As shown in Fig. 5b, the E_g of TiO_2 is estimated to be 3.1 eV, so TiO_2 is hardly photoexcited by visible light. The E_g of CuPDIsm and PDIsm are 1.91 and

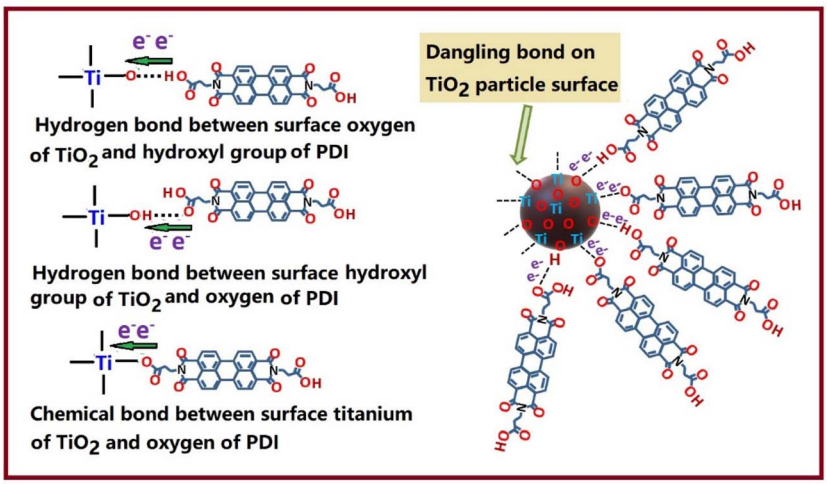

Fig. 4 Schematic illustration of binding interaction and charge transfer at the interface between PDIsm and TiO_2.

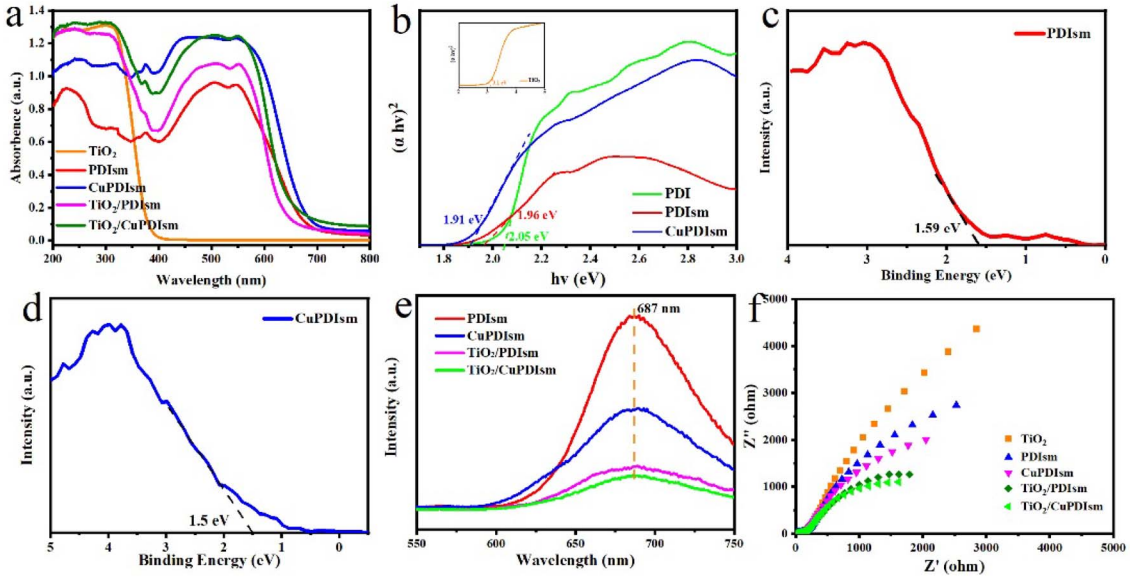

Fig. 5 UV-vis diffuse reflectance spectra of the samples (a) and the corresponding Tauc's plots (b), valence band potential diagrams of PDIsm (c) and CuPDIsm (d), photoluminescence profiles (e) and EIS profiles (f) of the samples.

1.96 eV, respectively, indicating their visible light photocatalytic activity. The valence band (VB) is determined as 1.59 eV for PDIsm and 1.5 eV for CuPDIsm by using XPS measurement (Fig. 5c and d). Thus, the conduction band (CB) of samples can be calculated according to the following equation:

$$E_{CB} = E_{VB} - E_g \quad (1)$$

the E_{CB} of PDIsm and CuPDIsm is determined as −0.37 and −0.41 eV, respectively.

Though PDIsm has good absorption of visible light and easily excited by visible light, its photocatalytic performance is still poor due to the high charge recombination.[7,14,15] Photoluminescence (PL) spectroscopy was used to measure the separation efficiency of photogenerated carriers (Fig. 5e). Compared with PDIsm, CuPDIsm has low luminescence intensity, proving its low charge recombination. This indicates that the metal–ligand interaction between adjacent PDI moleculars is more beneficial to the electron transfer than hydrogen bond link. Additionally, the mesoporous structure and high specific surface areas of CuPDIsm help to accelerate the migration of photo-generated electrons from the inside to surface as discussed above. TiO_2/CuPDIsm shows the lowest luminescence intensity among all the samples, which is attributed to the more efficient transfer of photogenerated charge through the hydrogen bond and C=O–Ti bond formed at the heterojunction interface.[50] The transfer efficiency of photogenerated electron was further investigated by the electrochemical impedance (EIS) spectra (Fig. 5f). The charge transfer resistance decreases in order: TiO_2 > PDIsm > CuPDIsm > TiO_2/PDIsm > TiO_2/CuPDIsm, further identifying that the conductivity is enhanced and electron transfer rate is accelerated when PDIsm is doped with copper and coupled with TiO_2. So, it can be concluded that the incorporation of Cu and TiO_2 with PDIsm not only expands the photo-absorption but also enhances the carrier separation efficiency, which were favorable for photocatalytic reaction.

3.3 Photocatalytic activity

TC, MO and MB were chosen as the target pollutants to investigate the photocatalytic activity of the samples. For anionic TC and MO organics (Fig. 6a and b), the photodegradation ratios of the samples increase in order: TiO_2 < PDIsm < CuPDIsm < TiO_2/PDIsm < TiO_2/CuPDIsm, so both Cu-doping and TiO_2 coupling can effectively increase the photocatalytic activity of PDIsm. TiO_2/CuPDIsm composites show the highest degradation ratios, reaching the maximum values of 89.87% toward TC and 68.65% toward MO. The excellent photodegradation efficiency of TiO_2/CuPDIsm is attributed to the noticeable photocharge transfer, high visible light absorption and large specific surface area as discussed above.

For cationic MB (Fig. 6c), TiO_2/CuPDIsm also shows excellent photodegradation ratio, reaching the maximum value of 97.26%. It is notable that the MB degradation curves of PDIsm and CuPDIsm almost overlap and the total MB adsorption finishes in the dark adsorption stage, indicating the strong adsorption ability of these two samples. To understand the adsorption capacity of PDIsm toward organic pollutants, the adsorption experiment was conducted using 20 mg of adsorbent in 40 mL of 300 mg L^{-1} MB for a duration of 9 h. In Fig. S5,† PDIsm shows much better adsorption capacity (528.7 mg g^{-1}) toward cationic MB, while poorer adsorption toward anionic TC and MO. The remarkable adsorption capacity toward cationic MB is attributed to the strong electrostatic attraction because PDIsm and CuPDIsm are negative charged with the ionization of abundant carboxyl groups in the aqueous solution. The high negative charge are identified by the zeta potential (Fig. S6†) of PDIsm (−85.15 mV) and CuPDIsm(−70.99 mV), so PDIsm and CuPDIsm have better

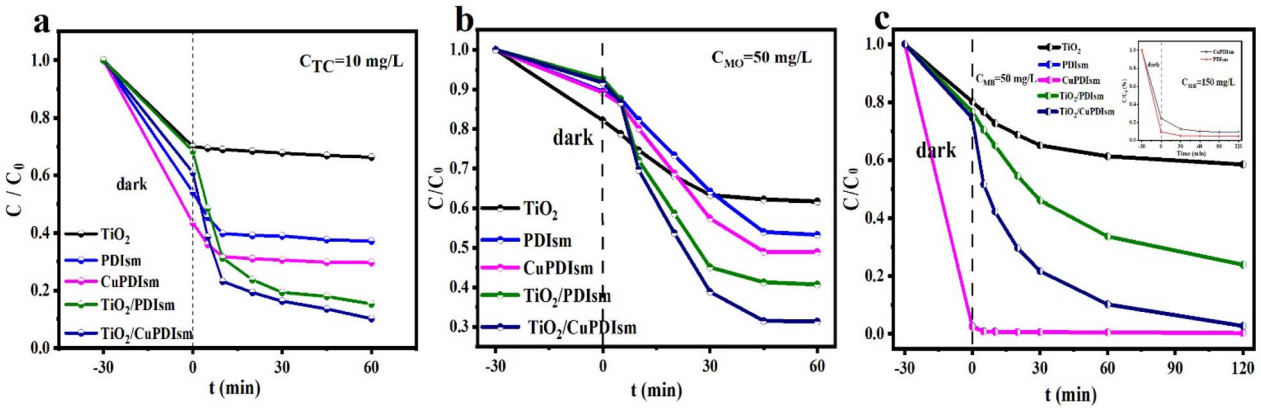

Fig. 6 The photodegradation ratios of the samples toward TC (a), MO (b) and MB (c).

adsorption ability toward cationic MB. However, it is difficult for anionic TC and MO to be adsorbed onto PDIsm and CuPDIsm surface due to the electrostatic repulsion. The excellent surface adsorption capacity is beneficial to enhancing the photo-performance of PDIsm and CuPDIsm based composites, explaining the better degradation ratio of PDIsm based composites toward MB than toward MO and TC.

The apparent rate constants of MO and MB were fitted by the pseudo-first-order equation (Fig. S7a and b†). CuPDIsm and TiO_2/CuPDIsm show higher K_{MO} than PDIsm and TiO_2/PDIsm, respectively, further proving that the photocatalytic activity of PDIsm can be effectively improved by Cu-doping and TiO_2-coupling. In addition, the cycling tests of TiO_2/CuPDIsm show that the degradation ratio of TC decreases slightly with the increase of cycle times and remains 71.45% after five cycles (Fig. S8a†). The XRD patterns (Fig. S8b†) show that the crystal structure of TiO_2/CuPDIsm hardly changes after the cycling experiment, indicating the good structural stability and favorable reusability of TiO_2/CuPDIsm.

3.4 Mechanism of photocatalytic activity

Radical trap experiment of TiO_2/CuPDIsm composites was performed to explore the photocatalytic mechanism. The isopropanol (IPA), benzoquinone (BQ) and ethylenediaminetetraacetic acid disodium (EDTA) were used as scavengers of $^{\bullet}OH$, $^{\bullet}O_2^-$ and h^+ species, respectively. As shown in Fig. 7a, the addition of IPA to the reaction system results in very limited change in the photodegradation of TC, MB and MO, indicating that $^{\bullet}OH$ plays a negligible role in the photodegradation reaction. The introduction of EDTA leads to a more significant decrease of the degradation efficiency than BQ addition, suggesting that the h^+ is identified as the main active species and $^{\bullet}O_2^-$ is the secondary active species. The ESR spin-trap experiment shows that the characteristic peaks corresponding to the DMPO/$^{\bullet}O_2^-$ adducts were detected (Fig. 7b) under visible light irradiation while no signals in dark, further implying that the $^{\bullet}O_2^-$ radicals are produced and involved in the photodegradation process. This indicates that the photoinduced electrons in TiO_2/CuPDIsm can be captured by dissolved oxygen to generate $^{\bullet}O_2^-$ radicals.[51,52] However, after 5, 10 and 20 min of light, the signal of DMPO–$^{\bullet}O_2^-$ was significantly enhanced. This indicated that the photoinduced electrons in TiO_2/CuPDIsm can be captured by O_2 to generate $^{\bullet}O_2^-$ radicals.[51]

The presence of the mainly generated species can also be theoretically inferred from valence band and conduction band of CuPDIsm. According to the obtained E_g (1.91 eV), E_{CB} (−0.41 eV) and E_{VB} (1.5 eV) of CuPDIsm as discussed above, $^{\bullet}O_2^-$ species can be generated because the E_{CB} of CuPDIsm was more negative than the reduction potential of O_2/$^{\bullet}O_2^-$ (−0.33 eV) and the photo-induced e^- can be captured by dissolved oxygen to form $^{\bullet}O_2^-$.[50,51] But very limited amount of $^{\bullet}OH$ species is generated since the E_{VB} of CuPDIsm is less positive than the oxidation potential of OH^-/$^{\bullet}OH$ (1.99 eV) and H_2O/$^{\bullet}OH$ (2.37 eV).[53] So, under visible light irradiation, PDIsm can be photoexcited and facilitates $^{\bullet}O_2^-$ and h^+ active species for the degradation of organic pollutants.

Though PDIsm can be theoretically photoexcited, it shows low photodegradation performance due to the low transport efficiency of photo-generated electrons, which depends on the migration path along the π–π long-range transport pathway with the hydrogen bond link between the carboxylic side chains. When Cu is doped into PDIsm, the hydrogen bond link is replaced by the stronger metal–ligand interaction between adjacent side chains and hence the electron transfer is greatly accelerated. Additionally, the mesoporous structure of CuPDIsm system can shortens the migration distance of electrons from inside to surface and so enhances the spatial charge separation. Moreover, when TiO_2 is coupled with CuPDIsm, surface hydrogen bond interaction (–C═O–H)[22] and electronic coupling interaction (C═O–Ti)[13,23] form at the heterojunction interface, which provide the fast-channel for the transfer of electrons from CuPDIsm to the reactive (101) surface and conduction band of TiO_2.[13,22,23] This substantial electron transfer from CuPDIsm to TiO_2 has been identified by the shift of Ti 2p peaks to low binding energy position, as shown in Fig. 7c. The photocatalytic mechanism of TiO_2/CuPDIsm composite is shown schematically in Fig. 7d. Therefore, we corroborate that the highly efficient photocatalysis of CuPDIsm/TiO_2 are ascribed to simultaneous introduction of Cu and TiO_2 with the great enhancement of charge separation.

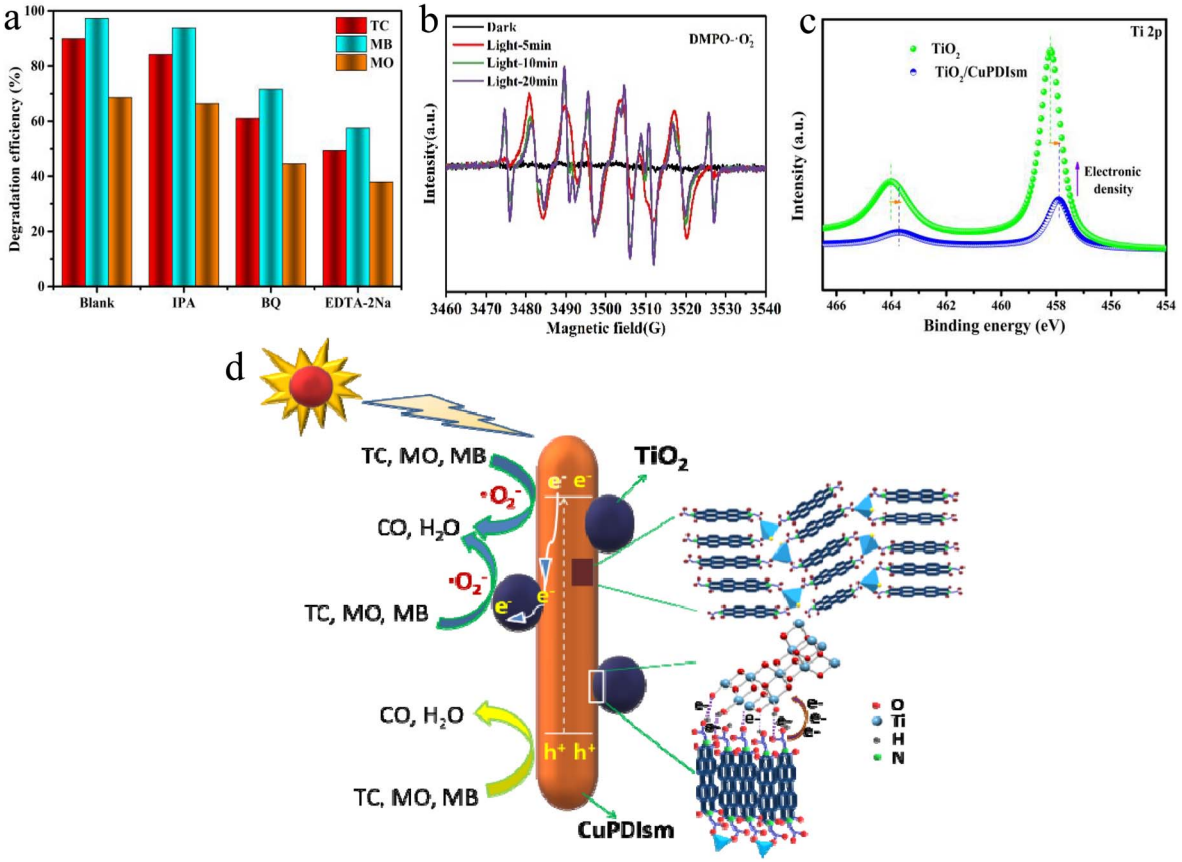

Fig. 7 Photodegration of TiO_2/CuPDIsm with the addition of scavengers (a), ESR spectra of TiO_2/CuPDIsm in aqueous dispersion for DMPO–$^{\bullet}O_2^-$ (b), high-resolution XPS of Ti 2p for TiO_2 and TiO_2/CuPDIsm (c), the photocatalytic mechanism of TiO_2/CuPDIsm composite (d).

4. Conclusion

We firstly prepared a novel CuPDIsm supramolecular by simple self-assembly of PDI moleculars in copper salt solution and then designed the TiO_2/CuPDIsm system with the growth of TiO_2 on CuPDIsm by hydrothermal method. CuPDIsm with mesoporous structure is constructed by face-to-face organization of molecular planes through H-type π–π stacking and edge-to-edge connects of molecular side-chains through metal–ligand interaction. TiO_2 is closely immobilized on CuPDIsm surface through –C═O–H and C═O–Ti links at the heterojunction interface. Both Cu-doping and TiO_2 coupling could forcefully not only increase the adsorption intensity of visible light but also accelerate the spatial carrier separation, and hence greatly promote the photodegradation performance under visible-light irradiation. TiO_2/CuPDIsm composites construct an efficient electron transport system and show remarkable photodegradation efficiency as comparison with pure TiO_2 and PDIsm, with the degradation ratios of up to 89.87%, 68.65% and 97.26% toward tetracycline, methyl orange and methylene blue, respectively. This work demonstrates a bright application prospect of inorganic–organic composite catalysts for environmental purification territory.

Conflicts of interest

The authors declare that they have no known competing financial interests or personal relationships that could have appeared to influence the work reported in this paper.

Acknowledgements

The authors gratefully acknowledge the financial support by National Natural Science Foundation of China (No. 11975212), Zhejiang Provincial Natural Science Foundation of China (No. LQY19A050001) and the Open Research Program of Engineering Research Center of Nano-Geomaterials of Ministry of Education (Grant No. NGM2020KF017).

References

1 X. Cheng, R. Guan, Y. Chen, Y. Sun and Q. Shang, The unique TiO_2(B)/$BiOCl_{0.7}I_{0.3}$-P Z-scheme heterojunction effectively degrades and mineralizes the herbicide fomesafen, *Chem. Eng. J.*, 2022, **431**, 134021.
2 B. Dai, J. Fang, Y. Yu, M. Sun, H. Huang, C. Lu, J. Kou, Y. Zhao and Z. Xu, Construction of infrared-light-responsive photoinduced carriers driver for enhanced

photocatalytic hydrogen evolution, *Adv. Mater.*, 2020, **32**, 1906361.

3 M. Shen, T. Ding, W. H. Rackers, C. Tan, K. Mahmood, M. D. Lew and B. Sadtler, Single-molecule colocalization of redox reactions on semiconductor photocatalysts connects surface heterogeneity and charge-carrier separation in bismuth oxybromide, *J. Am. Chem. Soc.*, 2021, **143**, 11393–11403.

4 Y. Zheng, Y. Chen, B. Gao, B. Lin and X. Wang, Phosphorene-based heterostructured photocatalysts, *Engineering*, 2021, **7**, 991–1001.

5 X. Liu, M. Sayed, C. Bie, B. Cheng, B. Hu, J. Yu and L. Zhang, Hollow CdS-based photocatalysts, *J. Materiomics*, 2021, **7**, 419–439.

6 Q. Zhang, L. Jiang, J. Wang, Y. Zhu, Y. Pu and W. Dai, Photocatalytic degradation of tetracycline antibiotics using three-dimensional network structure perylene diimide supramolecular organic photocatalyst under visible-light irradiation, *Appl. Catal., B*, 2020, **277**, 119122.

7 W. Wei, Z. Wei, D. Liu and Y. Zhu, Enhanced visible-light photocatalysis via back-electron transfer from palladium quantum dots to perylene diimide, *Appl. Catal., B*, 2018, **230**, 49–57.

8 A. S. Weingarten, R. V. Kazantsev, L. C. Palmer, M. McClendon, A. R. Koltonow, A. P. Samuel, D. J. Kiebala, M. R. Wasielewski and S. I. Stupp, Self-assembling hydrogel scaffolds for photocatalytic hydrogen production, *Nat. Chem.*, 2014, **6**, 964–970.

9 K. Yu, H. Zhang, C. Su and Y. Zhu, Visible-light-promoted efficient aerobic dehydrogenation of N-heterocycles by a tiny organic semiconductor under ambient conditions, *Eur. J. Org. Chem.*, 2020, **2020**, 1956–1960.

10 Q. Gao, J. Xu, Z. Wang and Y. Zhu, Enhanced visible photocatalytic oxidation activity of perylene diimide/g-C_3N_4 n–n heterojunction via π–π interaction and interfacial charge separation, *Appl. Catal., B*, 2020, **271**, 118933.

11 H. Wang, Y. Zhou, J. Wang, A. Li and P. François-Xavier Corvini, BiOBr/$Bi_4O_5Br_2$/PDI constructed for visible-light degradation of endocrine disrupting chemicals: synergistic effects of bi-heterojunction and oxygen evolution, *Chem. Eng. J.*, 2021, 133622.

12 S. Chu, Y. Pan, Y. Wang, H. Zhang, R. Xiao and Z. Zou, Polyimide-based photocatalysts: rational design for energy and environmental applications, *J. Mater. Chem. A*, 2020, **8**, 14441–14462.

13 Y. Li, X. Zhang and D. Liu, Recent developments of perylene diimide (PDI) supramolecular photocatalysts: a review, *J. Photochem. Photobiol., C*, 2021, **48**, 100436.

14 S. Chen, C. Wang, B. R. Bunes, Y. Li, C. Wang and L. Zang, Enhancement of visible-light-driven photocatalytic H_2 evolution from water over g-C_3N_4 through combination with perylene diimide aggregates, *Appl. Catal., A*, 2015, **498**, 63–68.

15 W. Wei and Y. Zhu, TiO_2@perylene diimide full-spectrum photocatalysts via semi-core-shell structure, *Small*, 2019, **15**, 1903933.

16 F. Zhang, W. Li, T. Jiang, X. Li, Y. Shao, Y. Ma and J. Wu, Real roles of perylene diimides for improving photocatalytic activity, *RSC Adv.*, 2020, **10**, 23024–23037.

17 W. Wei, S. Ouyang and T. Zhang, Perylene diimide self-assembly: From electronic structural modulation to photocatalytic applications, *J. Semicond.*, 2020, **41**, 091708.

18 H. Chen, W. Zeng, Y. Liu, W. Dong, T. Cai, L. Tang, J. Li and W. Li, Unique MIL-53(Fe)/PDI supermolecule composites: Z-scheme heterojunction and covalent bonds for uprating photocatalytic performance, *ACS Appl. Mater. Interfaces*, 2021, **13**, 16364–16373.

19 Z. Zhang, X. Chen, H. Zhang, W. Liu, W. Zhu and Y. Zhu, A highly crystalline perylene imide polymer with the robust built-in electric field for efficient photocatalytic water oxidation, *Adv. Mater.*, 2020, **32**, 1907746.

20 H. Ben, Y. Liu, X. Liu, X. Liu, C. Ling, C. Liang and L. Zhang, Diffusion-controlled Z-scheme-steered charge separation across PDI/BiOI heterointerface for ultraviolet, visible, and infrared light-driven photocatalysis, *Adv. Funct. Mater.*, 2021, **31**, 2102315.

21 Y. Zhang, D. Wang, W. Liu, Y. Lou, Y. Zhang, Y. Dong, J. Xu, C. Pan and Y. Zhu, Create a strong internal electric-field on PDI photocatalysts for boosting phenols degradation via preferentially exposing π-conjugated planes up to 100%, *Appl. Catal., B*, 2022, **300**, 120762.

22 W. Zeng, T. Cai, Y. Liu, L. Wang, W. Dong, H. Chen and X. Xia, An artificial organic-inorganic Z-scheme photocatalyst WO_3@Cu@PDI supramolecular with excellent visible light absorption and photocatalytic activity, *Chem. Eng. J.*, 2020, **381**, 122691.

23 X. Gao, K. Gao, X. Li, Y. Shang and F. Fu, Hybrid PDI/BiOCl heterojunction with enhanced interfacial charge transfer for a full-spectrum photocatalytic degradation of pollutants, *Catal. Sci. Technol.*, 2020, **10**, 368–375.

24 T. Cai, W. Zeng, Y. Liu, L. Wang, W. Dong, H. Chen and X. Xia, A promising inorganic–organic Z-scheme photocatalyst Ag_3PO_4/PDI supermolecule with enhanced photoactivity and photostability for environmental remediation, *Appl. Catal., B*, 2020, **263**, 118327.

25 W. Wei, D. Liu, Z. Wei and Y. Zhu, Short-range π–π stacking assembly on P25 TiO_2 nanoparticles for enhanced visible-light photocatalysis, *ACS Catal.*, 2016, **7**, 652–663.

26 X. Li, X. Lv, Q. Zhang, B. Huang, P. Wang, X. Qin, X. Zhang and Y. Dai, Self-assembled supramolecular system PDINH on TiO_2 surface enhances hydrogen production, *J. Colloid Interface Sci.*, 2018, **525**, 136–142.

27 Y. Wei, M. Ma, W. Li, J. Yang, H. Miao, Z. Zhang and Y. Zhu, Enhanced photocatalytic activity of PTCDI-C_{60} via π–π interaction, *Appl. Catal., B*, 2018, **238**, 302–308.

28 J. Yang, H. Miao, J. Jing, Y. Zhu and W. Choi, Photocatalytic activity enhancement of PDI supermolecular via π–π action and energy level adjusting with graphene quantum dots, *Appl. Catal., B*, 2021, **281**, 119547.

29 L. Zeng, T. Liu, C. He, D. Shi, F. Zhang and C. Duan, Organized aggregation makes insoluble perylene diimide efficient for the reduction of aryl halides via consecutive

visible light-induced electron-transfer processes, *J. Am. Chem. Soc.*, 2016, **138**, 3958–3961.

30 Z. Zhong, R. Li, W. Lin, X. Xu, X. Tian, X. Li, X. Chen and L. Kang, One-dimensional nanocrystals of cobalt perylene diimide polymer with insitu generated FeOOH for efficient photocatalytic water oxidation, *Appl. Catal., B*, 2020, **260**, 118135.

31 R. Singh, E. Giussani, M. M. Mróz, F. Di Fonzo, D. Fazzi, J. Cabanillas-González, L. Oldridge, N. Vaenas, A. G. Kontos, P. Falaras, A. C. Grimsdale, J. Jacob, K. Müllen and P. E. Keivanidis, On the role of aggregation effects in the performance of perylene-diimide based solar cells, *Org. Electron.*, 2014, **15**, 1347–1361.

32 B. Kaushik, D. Aniket, N. Tammene, H. Jialing, O. Randy, Y. Max, Z. Jincai and Z. Ling, Effect of side-chain substituents on self-assembly of perylene diimide molecules: morphology control, *J. Am. Chem. Soc.*, 2006, **128**, 7390–7398.

33 J. Wang, W. Shi, D. Liu, Z. Zhang, Y. Zhu and D. Wang, Supramolecular organic nanofibers with highly efficient and stable visible light photooxidation performance, *Appl. Catal., B*, 2017, **202**, 289–297.

34 D. Liu, J. Wang, X. Bai, R. Zong and Y. Zhu, Self-assembled PDINH supramolecular system for photocatalysis under visible light, *Adv. Mater.*, 2016, **28**, 7284–7290.

35 M. C. Nolan, J. J. Walsh, L. L. E. Mears, E. R. Draper, M. Wallace, M. Barrow, B. Dietrich, S. M. King, A. J. Cowan and D. J. Adams, pH dependent photocatalytic hydrogen evolution by self-assembled perylene bisimides, *J. Mater. Chem. A*, 2017, **5**, 7555–7563.

36 A. Datar, K. Balakrishnan and L. Zang, One-dimensional self-assembly of a water soluble perylene diimide molecule by pH triggered hydrogelation, *Chem. Commun.*, 2013, **49**, 6894–6896.

37 M. X. Zhang and G. J. Zhao, Modification of n-type organic semiconductor performance of perylene diimides by substitution in different positions: two-dimensional pi-stacking and hydrogen bonding, *ChemSusChem*, 2012, **5**, 879–887.

38 C. Xavier, C. Jérôme, F. Rainer, O. Koji Kamiya, L. Vincent, C. Annica, K. Gaël, L. Matthias, F. Mats, L. Roberto, G. Yves, W. Göran, U. Nobuo, B. Jean-Luc and R. S. William, Electronic delocalization in discotic liquid crystals: A joint experimental and theoretical study, *J. Am. Chem. Soc.*, 2004, **126**, 11889–11899.

39 M. Angelella, C. Wang and M. J. Tauber, Resonance Raman spectra of a perylene bis(dicarboximide) chromophore in ground and lowest triplet states, *J. Phys. Chem. A*, 2013, **117**, 9196–9204.

40 J. Yang, H. Miao, Y. Wei, W. Li and Y. Zhu, π–π Interaction between self-assembled perylene diimide and 3D graphene for excellent visible-light photocatalytic activity, *Appl. Catal., B*, 2019, **240**, 225–233.

41 A. Blacha-Grzechnik, A. Drewniak, K. Z. Walczak, M. Szindler and P. Ledwon, Efficient generation of singlet oxygen by perylene diimide photosensitizers covalently bound to conjugate polymers, *J. Photochem. Photobiol., A*, 2020, **388**, 112161.

42 E. K. Theo, D. Hao Wang, S. Vladimir and P. D. Frank Würthner, Supramolecular construction of fluorescent J-aggregates based on hydrogen-bonded perylene dyes, *Angew. Chem.*, 2007, **119**, 5637–5640.

43 Z. Chen, V. Stepanenko, V. Dehm, P. Prins, L. D. Siebbeles, J. Seibt, P. Marquetand, V. Engel and F. Wurthner, Photoluminescence and conductivity of self-assembled π–π stacks of perylene bisimide dyes, *Chem.–Eur. J.*, 2007, **13**, 436–449.

44 F. Wurthner, Z. Chen, V. Dehm and V. Stepanenko, One-dimensional luminescent nanoaggregates of perylene bisimides, *Chem. Commun.*, 2006, 1188–1190.

45 L. Yang, X. Hao, D. Yu, P. Zhou, Y. Peng, Y. Jia, C. Zhao, J. He, C. Zhan and B. Lai, High visible-light catalytic activity of bis-PDI-T@TiO_2 for activating persulfate toward efficient degradation of carbamazepine, *Sep. Purif. Technol.*, 2021, **263**, 118384.

46 S. Chen, Y. Xiao, Y. Wang, Z. Hu, H. Zhao and W. Xie, A facile approach to prepare black TiO_2 with oxygen vacancy for enhancing photocatalytic activity, *Nanomaterials*, 2018, **8**, 245.

47 Z. Zhuang, Y. Li, Z. Li, F. Lv, Z. Lang, K. Zhao, L. Zhou, L. Moskaleva, S. Guo and L. Mai, MoB/g-C_3N_4 interface materials as a Schottky catalyst to boost hydrogen evolution, *Angew. Chem., Int. Ed.*, 2018, **57**, 496–500.

48 Q. Ji, Z. Xu, W. Xiang, Y. Wu, X. Cheng, C. Xu, C. Qi, H. He, J. Hu, S. Yang, S. Li and L. Zhang, Enhancing the performance of pollution degradation through secondary self-assembled composite supramolecular heterojunction photocatalyst BiOCl/PDI under visible light irradiation, *Chemosphere*, 2020, **253**, 126751.

49 P. Karthik, T. R. Naveen Kumar and B. Neppolian, Redox couple mediated charge carrier separation in g-C_3N_4/CuO photocatalyst for enhanced photocatalytic H_2 production, *Int. J. Hydrogen Energy*, 2020, **45**, 7541–7551.

50 Z. Jiang, Y. Liu, T. Jing, B. Huang, Z. Wang, X. Zhang, X. Qin and Y. Dai, Enhancing visible light photocatalytic activity of TiO_2 using a colorless molecule (2-methoxyethanol) due to hydrogen bond effect, *Appl. Catal., B*, 2017, **200**, 230–236.

51 M. Ou, S. Wan, Q. Zhong, S. Zhang, Y. Song, L. Guo, W. Cai and Y. Xu, Hierarchical Z-scheme photocatalyst of g-C_3N_4@Ag/$BiVO_4$ (040) with enhanced visible-light-induced photocatalytic oxidation performance, *Appl. Catal., B*, 2018, **221**, 97–107.

52 P. Chen, L. Blaney, G. Cagnetta, J. Huang, B. Wang, Y. Wang, S. Deng and G. Yu, Degradation of ofloxacin by perylene diimide supramolecular nanofiber sunlight-driven photocatalysis, *Environ. Sci. Technol.*, 2019, **53**, 1564–1575.

53 S. Wang, D. Li, C. Sun, S. Yang, Y. Guan and H. He, Synthesis and characterization of g-C_3N_4/Ag_3VO_4 composites with significantly enhanced visible-light photocatalytic activity for triphenylmethane dye degradation, *Appl. Catal., B*, 2014, **144**, 885–892.